Cell Formation in Cylinder Wakes at Low Reynolds Numbers

T. Leweke,[1,2] M. Provansal,[1] G. D. Miller,[2] and C. H. K. Williamson[2]
[1]*Institut de Recherche sur les Phénomènes Hors Équilibre, UMR 6594 CNRS / Universités Aix-Marseille I & II, Faculté de Saint-Jérôme, Service 252, F-13397 Marseille Cédex 20, France*
[2]*Sibley School of Mechanical and Aerospace Engineering, Cornell University, Upson Hall, Ithaca, New York 14853-7501*
(Received 4 June 1996)

We propose a mechanism for the previously unexplained formation of spanwise cells observed in the vortex street wake of finite-length cylindrical bluff bodies at low Reynolds numbers. It involves the spatial growth of the secondary Eckhaus instability of oblique vortex shedding, controlled by end effects, and leads to a new interpretation of observed wake frequency relations. Predictions of cell size variations and wake patterns are obtained from the phenomenological Ginzburg-Landau model, and good agreement is found with experimental observations. [S0031-9007(97)02333-8]

PACS numbers: 47.27.Vf, 47.20.Ft, 47.20.Lz, 47.54.+r

A number of studies in recent years have investigated three-dimensional phenomena in the wake of two-dimensional bluff bodies, mainly circular cylinders, at low Reynolds numbers and have pointed out the importance of experimental end effects in creating some of the observed three dimensionalities (see the review in [1]). For cylinders, the Reynolds number is defined as $\mathrm{Re} = Ud/\nu$, where U is the free-stream velocity perpendicular to the cylinder, d the cylinder diameter, and ν the kinematic viscosity of the fluid. In the range $47 < \mathrm{Re} < 190$, the wake is periodic in time and takes the form of a regular street of alternating vortices. One of the observed features of this flow is the existence, under certain conditions, of a cellular structure of the wake in the spanwise direction [2,3]. In each cell the vortex shedding frequency has a different value, but is constant within one cell. At a given Reynolds number, the lowest frequency is found in the cells closest to the ends of the cylinder, first described by Gerich and Eckelmann [4]. The shedding frequencies associated with each cell increase from the end cell to the central cell of the wake. At the boundary between two cells a beat frequency from the two cell frequencies is measured and vortex dislocations are observed [2]. It was shown in [2] that the shedding frequency is linked to the angle θ between shed vortices and the cylinder, and that it is proportional to $\cos\theta$. This means that vortices in each cell are shed at a different angle, with the highest inclination in the end cells, which has been confirmed by the flow visualizations of König *et al.* [5]. The number and spanwise extent of the cells was found to depend on Reynolds number, cylinder aspect ratio, and end conditions [2,3]. While cellular shedding is known to occur in situations with nonuniform cylinder diameter or free-stream velocity, which can be understood by a spanwise coupling mechanism of the wake oscillations [6], little is known about the origin of cell formation in uniform conditions, i.e., away from the wall or end plate boundary layers in a circular cylinder setup. In this Letter we propose a mechanism of cell formation involving a secondary instability of oblique vortex shedding, first studied in detail for the case of a high-aspect ratio torus [7,8].

In straight cylinder wakes it was found that oblique vortex shedding becomes unstable, leading to a breakup into cells, when the shedding angle exceeds a critical value [2]. This phenomenon was also observed and studied more systematically in ring wakes [7,8], and it was shown that the critical angle θ_c for oblique (helical) vortex shedding is an increasing function of Reynolds number. This instability involves the excitation of sideband disturbances which result in an exponential growth of phase fluctuations. This leads to a growing modulation (waviness) of the vortex street pattern in time, until the initial pattern breaks down and a new state of vortex shedding with a lower, stable angle is reached. A detailed description can be found in [7,8]. Since the low curvature of the rings used in this study had only small quantitative effects on the wake dynamics, it can be expected that the same mechanism is acting in the straight cylinder wakes.

This secondary instability can be treated analytically with the help of the phenomenological Ginzburg-Landau (GL) model, which has been successfully used to describe the dynamics and spatial patterns in bluff body wakes at low Reynolds numbers [8–12]. In this model the velocity fluctuations in the near wake are assumed to be proportional to the real part of a complex amplitude $A(z,t)$, solution of the one-dimensional complex GL equation

$$\frac{\partial A}{\partial t} = \sigma(1 + ic_0)A + \mu(1 + ic_1)\frac{\partial^2 A}{\partial z^2} + l(1 + ic_2)|A|^2 A\,, \tag{1}$$

which describes the dynamics of a chain of coupled nonlinear oscillators along the spanwise direction z. The parameters in Eq. (1) are determined from experiments (see Refs. [7,8]). The values used for the present analysis take into account recent experimental findings reported in [12], in particular, concerning the important parameters c_1 and c_2, which are chosen here as $c_1 = -1.0$ and $c_2 = -3.0$.

Furthermore, the diffusive coupling parameter μ was allowed to vary with Re and was determined from frequency measurements and c_1 and c_2 as shown in [13]. In an infinite domain, and for supercritical conditions ($\sigma > 0$), Eq. (1) has plane wave solutions of the form

$$A(z,t) = M_Q \exp(i[\Omega_Q t + Qz]) . \tag{2}$$

Their amplitude M_Q and frequency Ω_Q depend on the spanwise wave number Q, which is equivalent to the shedding angle θ ([10], see also Eq. (6)). These waves represent parallel ($Q = 0$) and oblique ($Q \neq 0$) vortex shedding. Their stability is analyzed by introducing amplitude and phase perturbations, a and ϕ, in the form of Fourier modes,

$$A(z,t) = M_Q[1 + a(z,t)] \times \exp(i[\Omega_Q t + Qz + \phi(z,t)]) , \tag{3}$$

$$a(z,t) = a_0 \exp(\lambda t + iqz) , \quad \phi(z,t) = \phi_0 \exp(\lambda t + iqz) , \tag{4}$$

and solving the linearized perturbation equations for the complex growth rate $\lambda(Q,q) = \alpha(Q,q) + i\omega(Q,q)$ of the perturbations [8]. It is found that positive growth rates α can occur when Q exceeds a critical value $Q_c(\mathrm{Re})$. Figure 1 shows that the unstable perturbation wave numbers q lie in an interval around $q = 0$, whose size increases with Q. From plots like Fig. 1 one can determine the most unstable wave number q_m, and calculate its growth rate α_m and frequency from expressions given in Ref. [8]. In ring wakes the choice of the perturbation wave number is dictated by the periodic geometry [7,8]. Predictions for this case, derived from the above analysis, about the onset of the instability, its growth rate and frequency were found to be in very good agreement with experimental results. The analytical treatment using the Ginzburg-Landau model shows that this secondary instability is similar to the modulational or Eckhaus instability (see also Albarède and Monkewitz [10]), known from studies of spatial patterns in thin-layer cellular convection.

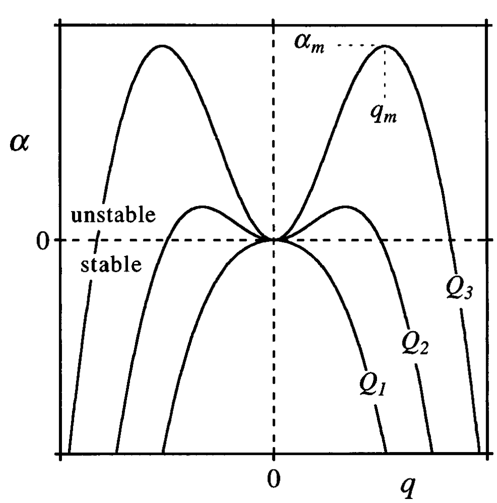

FIG. 1. Growth rates α of perturbations as a function of their wave number q for different wake wave numbers Q. $Q_1 < Q_c$, $Q_3 > Q_2 > Q_c$.

In spanwise uniform flow conditions, as in ring wakes or the idealized case of an infinite cylinder, the waviness resulting from the instability grows simultaneously along the entire span. This is expected to be different in the presence of localized end effects in the configuration considered here. Visualizations in [1] show that the flow at the cylinder ends can induce a strong inclination of the vortices, which then spreads into the central part of the wake due to the spanwise coupling of the wake oscillations, expressed in Eq. (1) by the diffusive term. From the low frequencies measured in the near-wall region it can be inferred that this inclination is above the Eckhaus stability limit. Furthermore, we can assume that the complicated flow at the ends also acts as a source of perturbations that can be amplified by the instability mechanism. Benjamin and Feir [14] pointed out that in such a case of a localized introduction of perturbations, these perturbations grow as they travel along the span away from their source; i.e., the growth is spatial and not temporal. Analytically, this can be described by replacing time t in the expression for the amplitude of the perturbations in Eq. (4), e.g., $\phi_0 \exp(\alpha t)$ for the phase, with z/c_g, where $c_g = |\omega/q|$ is the spanwise propagation speed of the modulation of the basic oblique shedding pattern, i.e., the group velocity of the combined basic (Q) and sideband (q) wave train [14]. The resulting phase distribution Φ of the latter has then the following form:

$$\Phi(z,t) = \Omega_Q t + Qz + \phi_0 \exp(z/l_0) \times \cos(\omega t + qz + \mathrm{const}) , \tag{5}$$

where the characteristic spanwise length for the growth of phase perturbations is given by $l_0 = c_g/\alpha = \alpha^{-1}|\omega/q|$. When the perturbation reaches a critical amplitude (ϕ_B, say), the vortices break up. If the spanwise location of this break is $z = B$, and the origin of z is chosen at the source of the perturbations (near the cylinder ends), then B is the size of the cell containing the unstable shedding angle. It is proportional to the characteristic length defined above: $B = \gamma l_0$, where the factor γ depends on the initial amplitude ϕ_0 at the source [$\gamma = \ln(\phi_B/\phi_0)$]. Park and Redekopp [9] have observed a similar breakup in numerical simulations using a two-dimensional GL equation and have determined the variation of cell size with model parameters and end conditions, but attributed the breakup into cells to the nonexistence of a global mode when the frequencies dictated by the ends are too low.

In the region where the "break" occurs, the perturbation amplitude is sufficiently large, so that the modulation frequency ω should be clearly detectable. This means that in our picture the "beat" frequency measured at the cell boundaries is due to the instability of the shedding pattern, and is not a result of the interaction between two patterns of different angles. On the contrary: the frequency of the pattern that is established on the other side of the break is due to the instability of the initial pattern alone.

The instability amplifies sideband disturbances, whose frequencies are combinations (sum and difference) of the initial and perturbation frequencies. Experimental observations show that the sideband mode with the higher frequency (lower shedding angle), being more stable than the other one, emerges after the break. The strong interaction between basic wave and perturbation in the break region can then be considered as a new "end" condition for the next cell, acting in turn as a source of perturbations that can be amplified and lead to another break in the pattern, if the new shedding angle is still above the stability limit. Thus the cell structure is built up by successive destabilization of oblique shedding patterns and is entirely determined by the initial angle and perturbation induced by the flow at the ends.

König *et al.* [3] have measured cell sizes in the wake of a cylinder bounded by wind tunnel walls. The spanwise wave number Q can be obtained from the measured frequency f or the angle θ of vortex shedding via the relation

$$Q = \frac{2\pi}{U_c} f_0 \sin\theta = \frac{2\pi}{U_c}(f_0^2 - f^2)^{1/2}, \tag{6}$$

which can be derived from simple geometric considerations [10] and the cosine dependence of the frequency on the shedding angle ($f = f_0 \cos\theta$) mentioned earlier [2]. f_0 is the wake frequency for parallel shedding at the same Reynolds number, and U_c the vortex convection speed, which is an approximately constant fraction of the free-stream velocity ($U_c/U \approx 0.9$) [2]. The most unstable wave number q_m is then calculated from the GL model as shown above, and the resulting predictions for the cell size B are compared in Fig. 2 to cell widths deduced from the measured cell boundary locations given in [3]. Here, only cells located entirely outside the wall boundary layer are considered, since it may be expected that the perturbation introduced by the cylinder/wall junction is not necessarily the most unstable one for the end cell shedding angle. Since the initial and breaking amplitudes, ϕ_0 and ϕ_B, are unknown, the factor γ has to be fitted; the present theory can only provide the shape of the curve. (The sensitivity of the result to the value of γ is illustrated in Fig. 3.) Nevertheless, Fig. 2 shows good agreement between the GL predictions and measurements. The unphysical zero crossing of the predicted X cell width is believed to be due to the simplified choice of the GL parameters. At lower Re their values differ from previous results [8,10,11], and this has a higher influence on the predictions for large-angle cells. Calculations with c_1 close to zero lead to more realistic predictions at these Re. We have further carried out experiments at a fixed Reynolds number Re = 120 showing the variation of cell size with shedding angle, which can be imposed on the wake by placing a small suction tube (visible in the lower left corner of Fig. 5) at different downstream distances behind the cylinder, near one of its ends [12,15]. The results are compared in Fig. 3 to the prediction from the GL description of the Eckhaus instability, again using measured shedding frequencies and Eq. (6). Because of the low amplitude of perturbations introduced by the suction-tube end condition, the factor γ is significantly higher than for the experiments considered above for Fig. 2. The two results agree well with each other and show that the further the angle of shedding is above the limit θ_c the smaller the cell size. It is surprising that the unstable shedding pattern can persist over a relatively large spanwise length before it breaks up.

Figure 4 shows a contour plot of the total phase Φ [Eq. (5)] after making the transformation $t = -x/U_c$ from time to downstream distance x. This represents a "visualization" of the wake with the body on the left and

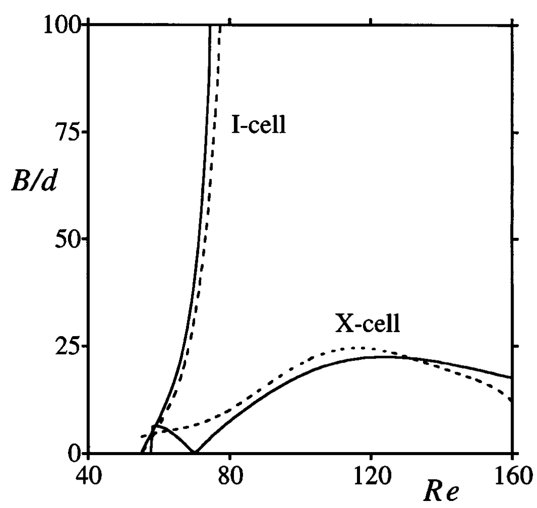

FIG. 2. Variation of cell size with Re. Experimental values deduced from Fig. 10 in [3] (dashed), and present GL prediction from the cells' frequency (solid), with $\gamma_I = 1$, $\gamma_X = 2.5$. I and X designate different cells in [3].

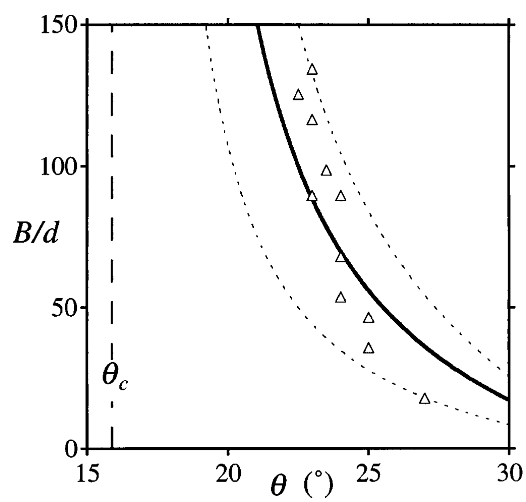

FIG. 3. Variation of cell size with shedding angle at Re = 120. Experiment (symbols) as shown in Fig. 5, and GL prediction (solid line) with $\gamma = 10$. The lower and upper dotted lines, corresponding to $\gamma = 5$ and $\gamma = 10$, respectively, show the influence of this parameter

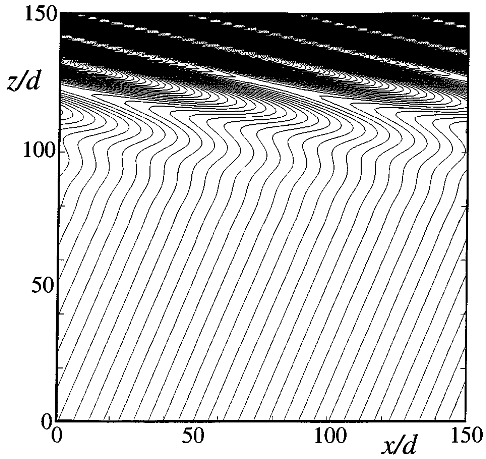

FIG. 4. Isophase lines of the GL amplitude A [from (5), with $t = -x/U_c$], showing the spatial development of the Eckhaus instability for $\theta = 23°$ at Re $= 120$.

flow from left to right (see Ref. [11]). A basic shedding mode with $\theta = 23°$ at Re $= 120$ was considered, which is destabilized by its most unstable perturbation having an arbitrarily chosen amplitude of $\phi_0 = 10^{-4}$ at $z = 0$. Again, it is striking that the waviness is barely visible over a span of almost 80 cylinder diameters and only shows up shortly before the break which is likely to occur around $z/d = 100$. While the pattern at the top of Fig. 4 depicts an unrealistically large amplitude, it demonstrates the modulation wave pattern. This result can be compared to the smoke visualization in Fig. 5 for the same Re and θ. (The initial perturbation amplitude ϕ_0 is, of course, unknown and may be different from the one assumed for Fig. 4.) The vortex pattern appears very similar to the one in Fig. 4, and the modulation waves, the sharply inclined smoke patterns in the break regions of the lower-end and central cells, can be clearly identified. The pattern after the break (at the top of Fig. 5) has a lower θ, and therefore a higher frequency.

The mechanism we propose for the formation of shedding cells in finite-cylinder wakes at low Reynolds numbers is the successive spatial destabilization of oblique shedding patterns by the Eckhaus instability, initiated at the ends. Good agreement is found between predictions of cell size variation and vortex street patterns, based on this mechanism, and experimental observations. In addition, our analysis suggests that, except for end cells, the frequency in each cell is completely determined by the shedding angle in its neighboring cell, and is given as the sum of the frequency of the latter and the frequency of its most unstable perturbation. This is conceptually different from the idea that the interaction between different oblique shedding patterns results in a low-frequency "beating" at the cell boundaries, an interpretation which would also not account for the origin of these patterns. The spatial character of the instability further explains the dependence of the cell structure on aspect ratio. The perturbations need room in the spanwise direction to reach an amplitude sufficient to break the pattern. If the cylinder is too short, unstable shedding angles may persist over the entire span, and fewer cells are observed than in the wake of a much longer cylinder.

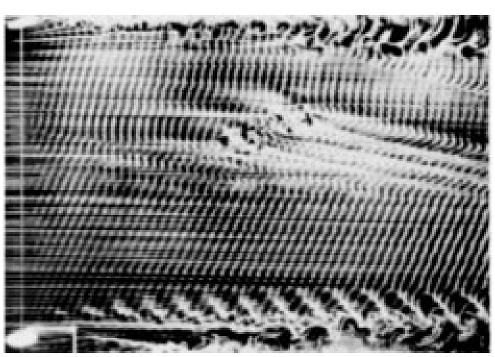

FIG. 5. Smoke visualization of a cylinder wake at Re $= 120$, with a shedding angle $\theta = 23°$ in the central span. Flow is from left to right. The waviness of this pattern and the modulation waves of the central and end cell patterns are clearly seen.

We gratefully acknowledge the financial support from the Deutsche Forschungsgemeinschaft under Grant No. Le 972/1-1 (T.L.), the "Action Incitative en Mécanique des Fluides" D.P.S.T. 8 of the French Ministère de l'Enseignement Supérieur et de la Recherche (M.P.), and the Office of Naval Research (G.D.M. and C.H.K.W.).

[1] C. H. K. Williamson, Annu. Rev. Fluid Mech. **28**, 477 (1996).
[2] C. H. K. Williamson, J. Fluid Mech. **206**, 579 (1989).
[3] M. König, H. Eisenlohr, and H. Eckelmann, Phys. Fluids A **2**, 1607 (1990).
[4] D. Gerich and H. Eckelmann, J. Fluid Mech. **122**, 109 (1982).
[5] M. König, H. Eisenlohr, and H. Eckelmann, Phys. Fluids A **4**, 869 (1992).
[6] B. R. Noack, F. Ohle, and H. Eckelmann, J. Fluid Mech. **227**, 293 (1991); A. Papangelou, *ibid.* **242**, 299 (1992).
[7] T. Leweke, M. Provansal, and L. Boyer, Phys. Rev. Lett. **71**, 3469 (1993).
[8] T. Leweke and M. Provansal, J. Fluid Mech. **288**, 265 (1995).
[9] D. S. Park and L. G. Redekopp, Phys. Fluids A **4**, 1697 (1992).
[10] P. Albarède and P. A. Monkewitz, Phys. Fluids A **4**, 744 (1992).
[11] P. Albarède and M. Provansal, J. Fluid Mech. **291**, 191 (1995).
[12] P. A. Monkewitz, C. H. K. Williamson, and G. D. Miller, Phys. Fluids **8**, 91 (1996).
[13] T. Leweke and M. Provansal, Europhys. Lett. **27**, 655 (1994).
[14] T. B. Benjamin and J. E. Feir, J. Fluid Mech. **27**, 417 (1967).
[15] G. D. Miller and C. H. K. Williamson, Exp. Fluids **18**, 26 (1994).